

Reduction and Sulfidation Kinetics of Cerium Oxide and Cu-Modified Cerium Oxide

Makoto Kobayashi[†] and Maria Flytzani-Stephanopoulos*

Department of Chemical and Biological Engineering, Tufts University, Medford, Massachusetts 02155

The reducibility and H₂S absorption capacity of cerium oxide and Cu-containing cerium oxide were examined in this work in the temperature range 623–923 K. The sorbents, prepared in bulk oxide form by the urea coprecipitation/gelation method, were composed of a cerium oxide backbone with a small amount of copper (5–40 atom %). Kinetics testing was conducted in a TGA apparatus. Temperature-programmed-reduction (TPR) experiments and *in situ* X-ray diffraction analysis were used to determine the reduction temperature and the various metal/oxide crystal phases. CuO in ceria was reduced to Cu metal at temperatures below 453 K. The reducibility of cerium oxide was increased by the presence of copper. A low Cu content (5 atom %) was sufficient to cause surface reduction of ceria at a temperature as low as 423 K. Sulfidation of prereduced samples was performed at 0.1 MPa in H₂S–H₂–N₂ gas mixtures. The contribution of reduced cerium oxide to sulfidation was evident even at the low temperature 623 K. Thus, copper promotes both the reducibility and sulfidation of cerium oxide. The activation energy of the sulfidation reaction was calculated from initial sulfidation reaction rates over the temperature range 623–923 K. A low apparent activation energy of 16 ± 3 kJ/mol was found for the Cu contents 5 and 15 atom % in ceria, while the activation energy is 34 kJ/mol for the 40 atom % Cu–CeO_x sorbent. This work has shown that copper-modified cerium oxide can be used as a sulfur sorbent over a wide temperature window.

Introduction

Sulfidation kinetics of bulk oxides^{1–3} and mixed metal oxides^{4–7} have been reported in the literature, primarily in connection with the application of these materials to high-temperature desulfurization of coal-derived gas streams. Mixed metal oxide combinations have been examined with the aim of stabilizing or promoting the reactivity, absorption capacity, or regenerability of one of the component oxides.^{4–7} Thus, oxides of iron, aluminum, titanium, or chromium have been used as additives to ZnO or CuO to improve the performance of the latter oxides in cyclic sulfidation/regeneration at high temperatures (550–800 °C).

A major issue with ZnO is its reducibility. While reduction of ZnO is very slow at temperatures below 500 °C, any zinc that might form is immediately vaporized above 400 °C.^{8,9} Zinc migration to and agglomeration on the surface of ZnO-containing sorbent particles is thus possible.^{10–12} This progressive structural modification has been found detrimental for regenerative application of ZnO-based sorbents to hot gas cleanup.¹³ Titanium dioxide has been used with ZnO to form zinc titanates of lower reducibility.^{10,11} However, the sulfidation activity of zinc titanate compounds, for example, Zn₂TiO₄, ZnTiO₃, and so forth, is also lower than that of ZnO.^{5,11}

Unlike the case of zinc oxide, CuO reduction to the metallic state occurs readily in the highly reducing coal gas atmosphere; however, the vapor pressure of metallic

copper is negligible. The problem with metallic copper is its low sulfidation equilibrium constant, which is several orders of magnitude lower than that of CuO or Cu₂O.^{8,9} There have been several attempts in the literature to stabilize CuO against reduction by combining it with other oxides, such as Al₂O₃,^{7,12,14} Fe₂O₃,^{12,14} or Cr₂O₃^{15,16} in order to improve its H₂S removal efficiency.

In previous work in this lab,¹⁶ CuO was mixed with cerium oxide, CeO₂, in an attempt to improve the properties of the former for high-temperature coal gas desulfurization. Interestingly, CeO₂ does not form a compound oxide with copper. In fact, ceria enhances the reducibility of copper oxide,^{17,18} a portion of which exists as highly dispersed clusters in ceria. The CuO–CeO₂ system, containing equal molar parts of CuO and CeO₂, was found to be a very efficient sorbent for high-temperature gas desulfurization.^{15,16} The sulfur capacity of CuO–CeO₂ is much higher than that corresponding to complete sulfidation of all the Cu in the composite, thus manifesting the contribution of cerium oxide. The H₂S removal efficiency of the Cu–CeO_x sorbent was also much higher than that of metallic copper, indicating the presence of a phase with a higher sulfidation equilibrium constant. This, we now believe, was due to part of the ceria being present as Ce₂O₃. The sulfidation and reduction kinetics of equimolar CuO–CeO₂ over the temperature ranges 723–1123 K and 823–1123 K, respectively, was reported in ref 16.

Cerium oxide has been much less examined than ZnO or CuO as a sulfidation sorbent. In its higher oxidation state (4+), cerium oxide has low sulfidation equilibria, but the reduced oxide, Ce₂O₃, is a superior H₂S sorbent.^{19–21} Recently, ceria was again evaluated as a high-temperature regenerable desulfurization sorbent, which yields elemental sulfur during regeneration.²²

* Corresponding author. E-mail: maria.flytzani-stephanopoulos@tufts.edu.

[†] Present address: Yokosuka Research Laboratory, Central Research Institute of Electric Power Industry, Nagasaka 2-6-1, Yokosuka 240-01, Japan.

A good way to increase the reducibility of ceria is to dope it with rare earth oxides or zirconia-forming oxide solid solutions with higher oxygen storage capacity (OSC) values than those for undoped ceria.^{23,24} Doped ceria is used to keep a stoichiometric air/fuel ratio in the automobile three-way catalyst, by releasing/accepting oxygen under fuel-rich/lean conditions in the exhaust gas stream. Higher ceria reducibility and OSC result by also incorporating platinum metal on the ceria-zirconia matrix.²⁵⁻²⁸ Recent work in this laboratory has found that Au or CuO additives in ceria have a similar effect on the reducibility and the OSC of ceria.^{18,29-31} Thus, the effect is more general and not limited to platinum metals on ceria. This opens up the application of ceria-based catalysts and sorbents to a wide variety of industrial processes, where more economical active catalysts are being sought. Transition metal-ceria systems have been recently demonstrated as active catalysts for several redox reaction systems of industrial interest, including the reduction of SO₂ to elemental sulfur,^{32,33} the partial oxidation of methane to syngas,³⁴ and the water-gas shift reaction.^{29-31,35}

On the basis of these findings, a suitably modified cerium oxide with metal oxide additives can be reduced more extensively to the Ce(III) oxide form, which has a large sulfidation equilibrium constant. If the kinetics of sulfidation is also fast, such a formulation may be one of the most attractive H₂S sorbents, with a much wider operating temperature window than is currently considered possible for cerium oxide. This paper reports on the reducibility and H₂S reactivity of copper-containing ceria in the temperature range 623–923 K.

Experimental Procedures

Sorbent Preparation. Cerium(IV) oxide and copper-containing cerium oxide were prepared by the urea precipitation gelation method from aqueous solutions of inorganic salts.^{18,36} The raw materials were ammonium cerium(IV) nitrate (Aldrich Chemical Co., Inc.) and copper(II) nitrate trihydrate (Johnson Matthey Electronics). To prepare the 5 atom % copper-ceria, 13.7 g of ammonium cerium nitrate and 0.3 g of copper nitrate were dissolved in 200 mL of deionized water and mixed so that the atomic ratio of Ce/Cu was 0.95:0.05. The same amount of ammonium cerium nitrate and deionized water was used for bulk cerium oxide preparation. Each solution was then subjected to precipitation reactions. The precipitant was ammonia produced by the hydrolysis of urea (Aldrich Chemical Co., Inc.). Excess (24 g) urea was added to the mixture. The flask containing the solution was continuously stirred with a magnetic stirrer on a hot plate so that the solution kept boiling. After the precipitate was observed, deionized water was added to the solution to a total volume of 500 mL. The solution was kept boiling for 6 h. The precipitate was then filtered, washed in deionized water twice, dried in a vacuum at 373 K for 16 h, and crushed to a powder before calcination. It was then placed in a porcelain crucible and calcined at 923 K in static air for 20 h in a muffle furnace. A slow heating rate of 2 K/min was used to the final calcination temperature. The product was crushed and sieved through standard sieves. Particles of diameter less than 53 μm were used in the reactivity tests.

Thermobalance Reactor Tests. A thermogravimetric analyzer assembly (Cahn Instruments, TGA-113) was used to conduct temperature-programmed reduc-

Table 1. Conditions for Reduction and Sulfidation Tests

	reduction	sulfidation
temp (K)	623–1023	623–1023
pressure (MPa)	0.10	0.10
gas composition (vol %)	H ₂ , 10.0 N ₂ , balance	H ₂ , 10.0 H ₂ S, 1.0 N ₂ , balance
gas flow rate (L/min) (NTP)	0.30–0.70	0.30–0.70
sorbent particle size (μm)	<53	<53
sorbent weight (mg)	4–10	4–10

tion (TPR) tests and to measure the sulfur uptake of various CuO–CeO_x compositions. The electrobalance (Cahn, C-2000) and furnace temperature controller (Micron, 823) were used as originally supplied, while the data acquisition system was replaced with a PC equipped with a 12 bit analog/digital converter (Omega Engineering, Inc., WB-ASC-TC). The gas flow rate was controlled by mass flow controllers (Brooks, Model 5850) and supplied to the TGA at 0.10 MPa. Reaction temperatures and gas compositions are shown in Table 1. A 5% H₂–N₂ gas mixture was used as the reductant gas in the TPR tests. Sulfidation was studied with the same reducing gas, also containing hydrogen sulfide. Hydrogen sulfide was introduced in the reducing gas by replacing nitrogen with the corresponding flow rate of a H₂S–N₂ gas mixture. Temperature was raised at a constant rate of 10 K/min. The sample powder was spread on quartz wool that filled a hemispherical quartz pan suspended by a thin quartz hangdown wire. The sample was first heated in N₂ gas flow at 650 °C and then cooled to the desired test temperature. All procedures, which included temperature variation and gas composition variation, were calibrated by blank tests to compensate for the effect of buoyancy and apparent flow rate change. The sample weight was determined from the difference between the weight variations in the actual test and the calibration run. Kinetic data for both the reduction and sulfidation tests were obtained in another TGA setup (Cahn Instruments, TG-151) consisting of a quartz tube of 34.5 mm i.d. The sorbent powder was spread on a flat filter (1.2 cm² area) made of quartz fiber. A load of 4–10 mg was used. The filter was laid on the sample pan. The gas flow rate was 500 cm³/min in the kinetics tests. Gas compositions are shown in Table 1.

Sorbent Characterization and Chemical Analysis. Specific surface areas of the prepared and used sorbents were determined by the BET-N₂ method using a flow BET apparatus (Micromeritics, Pulse ChemiSorb 2705). The pore size distribution of the oxides up to 100 nm was determined by nitrogen adsorption using an automatic BET instrument (BEL Japan, Inc., Belsorp 36). The crystal structure was determined from the diffraction pattern obtained with a X-ray diffractometer (MAC Science, Co., Ltd., MXP18VAHF22-SRA) equipped with a high-temperature sample stage. This sample stage permits *in situ* measurements under reducing conditions at ambient pressure. A rotating copper or molybdenum anode tube was used to determine the crystal structure of copper-containing samples and unmodified cerium oxide samples, respectively.

Results and Discussion

Thermodynamic Considerations. The reduction and sulfidation equilibria of CuO are well established.^{8,9,37,38} CuO is readily reduced to the metal state,

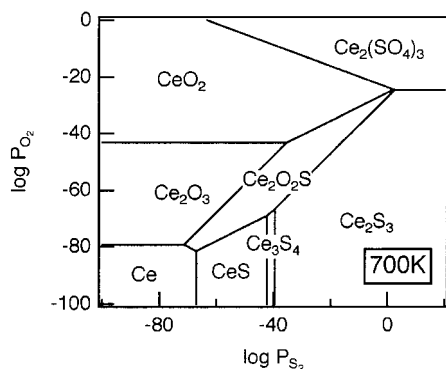


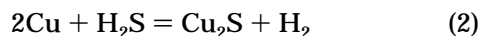
Figure 1. Phase diagram of the Ce–O–S system at 700 K.^{8,9,41}

while Cu_2O exists only when the partial pressure of oxygen exceeds 10^{-10} atm at 1000 K. The sulfidation product of copper is cuprous sulfide, Cu_2S , under the experimental conditions used here. The Cu–O–S phase diagram was included in a recent paper.³⁹ Reactions 1 and 2 below are the reduction of CuO and sulfidation of Cu, respectively. For the Ce–O–S system, phase stability diagrams were produced at temperatures above 1000 K by Kay and Wilson.⁴⁰ Here, we have used thermodynamic data from Barin et al.^{8,9} to draw the Ce–O–S phase diagram at 700 K, as shown by Figure 1. A very reducing atmosphere is required to produce the cerous oxide, Ce_2O_3 , from ceria. Cerium oxysulfide, $\text{Ce}_2\text{O}_2\text{S}$, is stable, and its thermodynamic constant at high temperature has been determined experimentally using the galvanic cell technique.⁴¹ Because the Gibbs free energy of the oxysulfide is given above 1073 K, the data required for Figure 1 were extrapolated to 700 K. The other possible products are various cerium sulfides, as shown in the phase diagram of Figure 1. Cerium oxysulfide and cerous sulfide can be derived from both cerium(IV) oxide (reactions 4 and 6) and cerium(III) oxide (reactions 5 and 7).

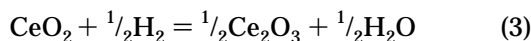
Reduction of Copper(II) Oxide



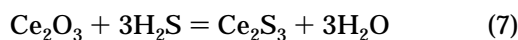
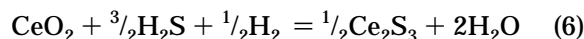
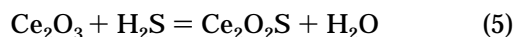
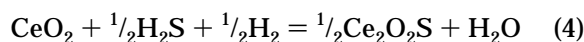
Sulfidation of Copper



Reduction of Cerium(IV) Oxide



Sulfidation of Cerium Oxide



Characterization of Cerium Oxide and Copper-Containing Cerium Oxide. All samples prepared in this work contained cerium(IV) oxide, as identified by XRD; see Figure 2. CeO_2 crystallizes in the face-centered cubic system and has a characteristic fluorite oxide-type structure. The diffraction pattern was rather broad, indicating a small crystallite size of the oxide phase. The Warren and Averbach method⁴² was used to estimate

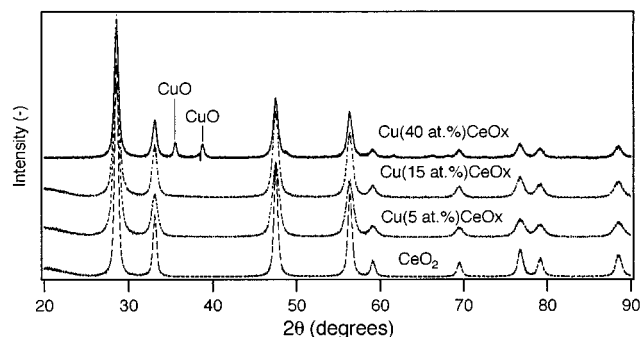


Figure 2. XRD chart of Cu (5–40 atom %)- CeO_x and CeO_2 powders after the air-calcination step.

the crystallite size of ceria from the half-height width of each diffraction peak. This method is believed to be the most accurate and reliable in determining the crystallite size of a polycrystalline material with a strained lattice.⁴² Data analysis of the X-ray diffraction pattern showed that the average crystallite size of the unmodified cerium oxide was 12.8 nm. This value is smaller than the value of 20.1 nm estimated from the measured specific surface area ($41.3 \text{ m}^2/\text{g}$) of this sample. The Warren and Averbach method estimates smaller crystallite sizes compared to those from other methods.⁴² Another possible reason for the difference may be the existence of closed pores.

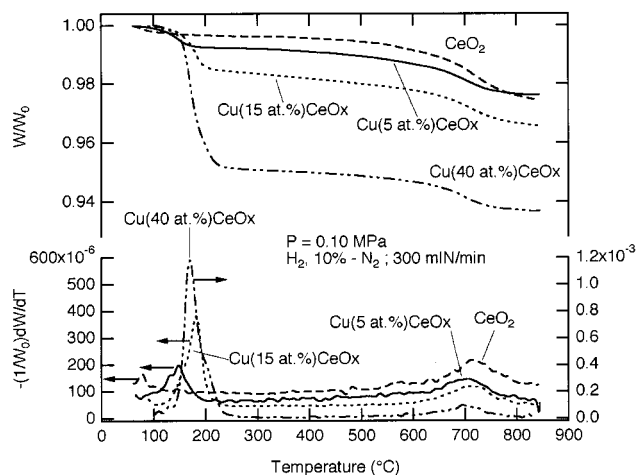
The crystallite sizes obtained by XRD for copper-modified cerium oxide were smaller than those of pure ceria, as shown in Table 2. The surface area is maximum for the low-content 5 atom % Cu- CeO_x sample, which also has the smallest ceria crystallite, 7 nm. When the copper content is higher than 15 atom %, growth of CuO crystals is observed (Figure 2), but the ceria crystallites remain small, probably as a result of enrichment of the grain boundaries with copper oxide.⁴³ No copper oxide reflections were found by XRD for copper contents lower than 15 atom %; see Figure 2. This indicates that copper oxide exists in a highly dispersed form. The existence of such a dispersed copper oxide phase of <3 nm particle size has been confirmed by STEM/EDS.⁴⁴ With Cu contents of 15 atom % or higher, bulk CuO particles (>40 nm) were present in addition to the dispersed clusters of copper oxide.^{44,45}

As shown in Table 2, pore closure and surface area loss were found for the high-content Cu-ceria samples. Typical type IV isotherms were obtained from nitrogen adsorption tests on the Cu- CeO_x samples. The hysteresis loop at relative pressures between 0.4 and 0.75 is of “type D”, indicating the existence of bottleneck-type pores.⁴⁶ The Dollimore–Heal method was applied to the isotherms of the desorption branch for determination of the pore size distribution of these samples between 2 and 60 nm. In this size range, all samples had an isolated pore size distribution whose peak diameter was 3.8 nm. The pore volume of each sample, however, varied as shown in Table 2. Pore plugging may have occurred in the high-content Cu-ceria samples during the calcination step.

Reduction Characteristics of Cerium(IV) Oxide. Reduction of pure cerium(IV) oxide was examined and used as a benchmark. H_2 -TPR of ceria was performed in the TGA from room temperature to 1123 K in 10 vol % H_2/N_2 . Appreciable reduction begins at temperatures above 923 K, as shown in Figure 3. This figure shows the sample weight variation together with its derivative function. If all the cerium(IV) oxide were reduced to

Table 2. Characterization of Fresh Sorbents

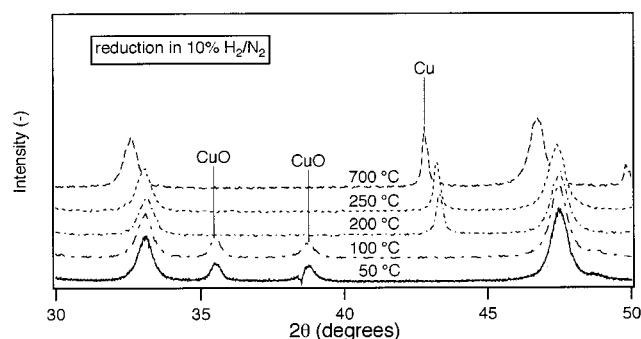
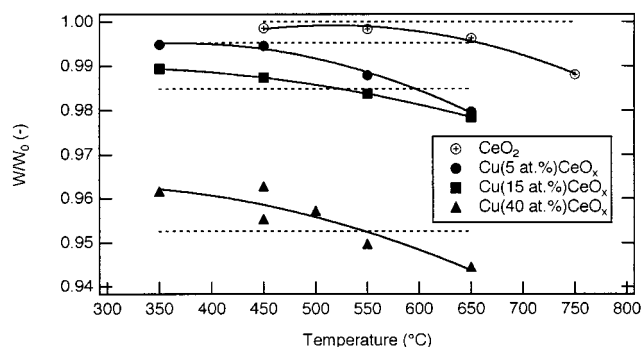
sorbent	BET surface area (m ² /g)	pore volume for 2–60 nm (cm ³ /g)	crystallite size of CeO ₂ (nm)	XRD identified phase
CeO ₂	41.33	0.065	12.8	CeO ₂ , fluorite structure
Cu _{0.05} CeO _x	63.03	0.098	7.2	CeO ₂ , fluorite structure
Cu _{0.15} CeO _x	32.27	0.055	8.8	CeO ₂ , fluorite structure
Cu _{0.40} CeO _x	19.97	0.040	9.6	CeO ₂ , fluorite structure and CuO

**Figure 3.** H₂-TPR profiles of CeO₂ and Cu–CeO_x samples.

Ce₂O₃, the weight ratio, W/W_0 , would fall to 0.95. A very small weight change, <0.5%, is observed at low temperatures, beginning around 500 K, in agreement with other reports.^{18,24–26} This reflects the reduction of the surface oxygen of ceria, while the high-temperature reduction is that of the bulk oxygen. We have reported elsewhere that when ceria is doped with La₂O₃, the amount of surface oxygen is increased, and a higher extent of reduction is measured at low temperatures.^{18,30}

Reducibility of Cu–CeO_x. In this work, undoped ceria was used, so that we could study the effect of CuO addition on the reducibility and the sulfur capacity of ceria. Although the copper phases in the low-content Cu samples could not be identified by XRD, we can reasonably assume most copper to be present as Cu(II) oxide from the previous thermodynamic considerations. Evidence for coexistence of the Cu(I) form also exists in the literature.⁴⁴ The reduction of CuO to Cu (eq 1) was assumed in our (conservative) calculations of ceria reducibility reported below.

Figure 3 shows the H₂-TPR of copper-containing ceria. In the sample with atomic ratio of Cu/Ce = 5:95, the derivative plot of the profile shows a weight decrease that has a peak at around 423 K. This weight decrease was not present in the TPR of pure cerium(IV) oxide shown in the same figure. This peak mainly corresponds to reduction of copper oxide.^{17,18} However, the weight decrease up to 573 K is larger (7.5×10^{-3}) than the value of 5.0×10^{-3} expected from complete reduction of CuO. This is attributed to enhanced surface reduction of ceria caused by the presence of copper, similar to what has been reported for the platinum metals and ceria interaction.^{24–26} The reduction of the 15 atom % Cu–CeO_x sample was similar, except that the low-temperature peak shifted to ~453 K. Figure 3 also shows the TPR of ceria containing 40 atom % Cu. The weight loss up to 573 K is 5.0×10^{-2} , which corresponds well to the reduction of CuO to metallic copper. Excess weight decrease from ceria is very hard to notice in this sample because of the large contribution from CuO. As the copper(II) oxide phase in this sample was identified

**Figure 4.** *In situ* XRD of Cu (40 atom %)–CeO_x reduced in a 10% H₂/N₂ gas mixture at various temperatures.**Figure 5.** Weight decrease due to reduction of Cu (5–40 atom %)–CeO_x in a 10% H₂/N₂ gas mixture after the initial 300 s of reduction at various temperatures. Horizontal lines show the W/W_0 value for complete reduction of the CuO portion of each sorbent.

by XRD (Figure 2), its reduction product was determined by an *in situ* XRD measurement. As shown in Figure 4, the CuO phase was reduced to Cu at temperatures between 373 and 423 K. The reduction peak temperature due to reduction of copper oxide increased by 80 K compared to that of the low-copper-content ceria. However, the reduction temperature is still lower than the temperature of 553 K reported for reduction of supported copper oxide.⁴⁷

CeO₂ reduction occurs simultaneously with CuO reduction even at temperatures below 473 K.^{18,29–31} Reduction experiments were also run under isothermal conditions. The contribution of ceria to the amount of oxygen removed from the sorbent was compared as a function of copper content, as shown in Figure 5. The extent of reduction was calculated from the W/W_0 –time profile at 300 s of reduction for all sorbent compositions. While reduction is not complete after 300 s, the plot clearly shows the contribution of ceria reduction. Complete copper oxide reduction is shown by the dotted lines in Figure 5. The greatest relative effect is shown by the 5 atom % Cu–CeO_x sample.

The overall sorbent reduction was examined for the three Cu-containing ceria samples in the temperature range 350–650 °C over 10 min. Conversion of CuO, X_{r1} , was first calculated assuming reduction of only the copper oxide phase. The value X_{r1} may exceed unity because of contribution from ceria reduction. X_{r1} –time

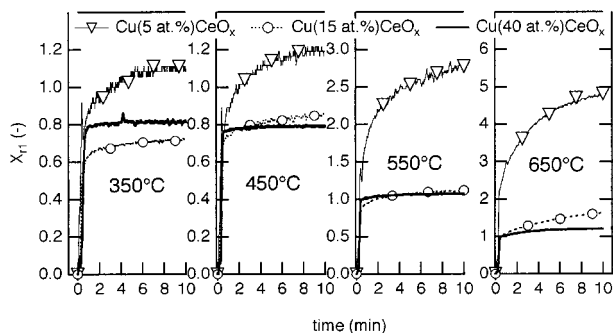


Figure 6. Conversion of CuO in reduction of Cu–CeO_x (10% H₂–N₂, 500 mL of N₂/min, 0.1 MPa).

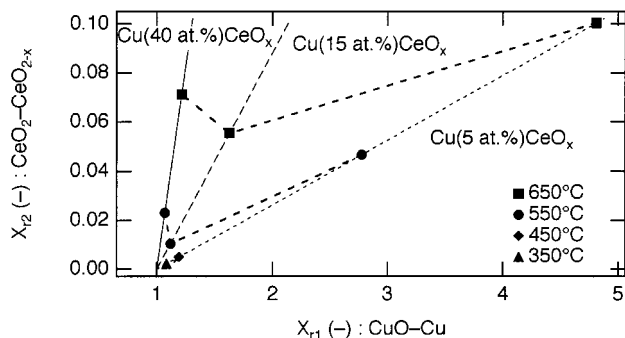


Figure 7. Estimated conversion of CeO₂ after 10 min of reduction of Cu–CeO_x samples at various temperatures.

plots are shown in Figure 6. The X_{r1} values exceed unity at all temperatures for 5 atom % Cu–ceria. At 650 °C, X_{r1} is ~ 5 for this sample at the end of the 10 min period. The values of X_{r1} are much lower for the other two sorbent compositions, even at high temperatures. From the profiles of Figure 6, one may be tempted to assign very fast kinetics to CuO reduction (to $X_{r1} = 1$) and slow kinetics to the excess reduction due to ceria. However, this may not be the case, as simultaneous reduction of both oxides can occur during the rapidly rising early reduction part of the process, where X_{r1} is below unity.

To evaluate the degree of ceria reduction as a function of copper loading, we need to convert the excess CuO conversion in Figure 6 to the corresponding reduction conversion of ceria, X_{r2} . Figure 7 shows the calculated conversion of ceria corresponding to the X_{r1} values for each of the three samples and for each of the four temperatures tested after 10 min of reduction. At each temperature, the extent of reduction of ceria is highest for the 5 atom % Cu–CeO_x sample. Conversion increases with temperature, as expected. Interestingly, in the sample containing 40 atom % Cu, the extent of ceria reduction is higher than that in the 15 atom % Cu–CeO_x sample. This finding is not understood in view of the physical properties of these two samples, as shown in Table 2, on the basis of which we would anticipate a higher ceria reducibility for the 15 atom % Cu–CeO_x sample. In more recent work with La-doped Cu–ceria,^{18,48} we have found the ceria reducibility to rank with its physical properties (surface area, crystallite size) and increase with copper loading up to 10–15 atom %. Thus, we attribute the anomalous behavior in Figure 7 to a peculiarity in the preparation of the present 15 atom % Cu–CeO_x sample which rendered it less dispersed than expected.

Initial Reduction Rates. In this section, the relatively rapid reaction observed at the beginning of the reduction, namely up to 100 s, is discussed in terms of

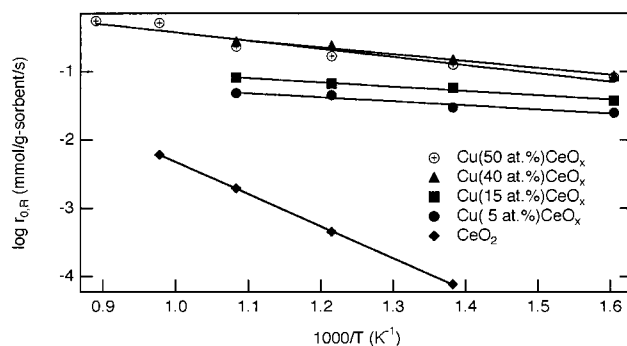


Figure 8. Arrhenius plot of initial reduction rate of CeO₂ and Cu (5–40 atom %)–CeO_x. Data for the equimolar Cu–ceria sample are from ref 16 (10% H₂/N₂, 500 mL of N₂/min, 0.1 MPa).

rate dependence on temperature and copper content. To ensure that rate measurements in the TGA were carried out in the absence of gas diffusion limitations, the effect of flow rate on the test results was evaluated. The flow rate effect on the initial reduction rate was negligible at values exceeding 500 mL of N₂/min. Thus, all kinetic tests were conducted at the flow rate 500 mL of N₂/min. Figure 8 shows Arrhenius-type plots of the initial reduction rates measured for each sorbent composition. Rates are expressed in millimoles of oxygen removed per gram of sorbent. Values for the initial reduction rate, $R_{r,0}$, were calculated from the slope of the W/W_0 –time profile at 10 to 12 s after switching in the H₂-containing gas in the TGA. This is the effective “zero” time for reduction, due to the change over of the system gas volume upon gas switching. As can be seen in Figure 8, the log plots of the initial reduction rates are linear and of much lower slope for the Cu–ceria samples than for neat ceria.

From the data of Figure 8, we calculated the reduction rate constants, k_r , by assuming a power-law dependence of the rate on the concentration of H₂, $R_{r,0} = k_r C_{H_2}^n$. The reaction order, n , was determined from a series of tests at 823 K in H₂ contents of 5–20 vol % in the gas mixture. This was equal to 0.78, a value close to that found in previous work for an equimolar CuO–CeO₂ sample.¹⁶ Assuming the value of n to be independent of temperature, the Arrhenius constants can now be calculated from $k_r = k_{r,0} \exp(-E_a/RT)$. The activation energy is 14.2 kJ/mol for the low-Cu-content ceria samples and 21.9 kJ/mol for the 40 atom % Cu–CeO_x sample. The latter is about the same as that of the equimolar CuO–CeO₂ sample,¹⁶ data which are included in Figure 8 for comparison. These samples contain both dispersed nanoparticles of copper oxide and bulk CuO particles, which are more difficult to reduce.

A clear finding from the initial reduction rate comparison is how much easier it is to reduce the composite Cu–CeO_x structure compared to the unmodified ceria. As shown in Figure 8, the latter has a higher activation energy of reduction as well as much lower initial reduction rates. These findings complement the TPR data of Figure 3 and strongly indicate the presence of some easily reducible oxygen species. All evidence points to the interfacial oxygen at the copper–ceria boundary as the active oxygen species. Thus, the presence of nanoparticles of Cu_xO in ceria increases the interfacial concentration of oxygen per unit area, while bulk CuO particles have negligible contact area with the ceria particles. The sample with 40 or 50 atom % Cu still has a fraction of Cu present as nanoparticles

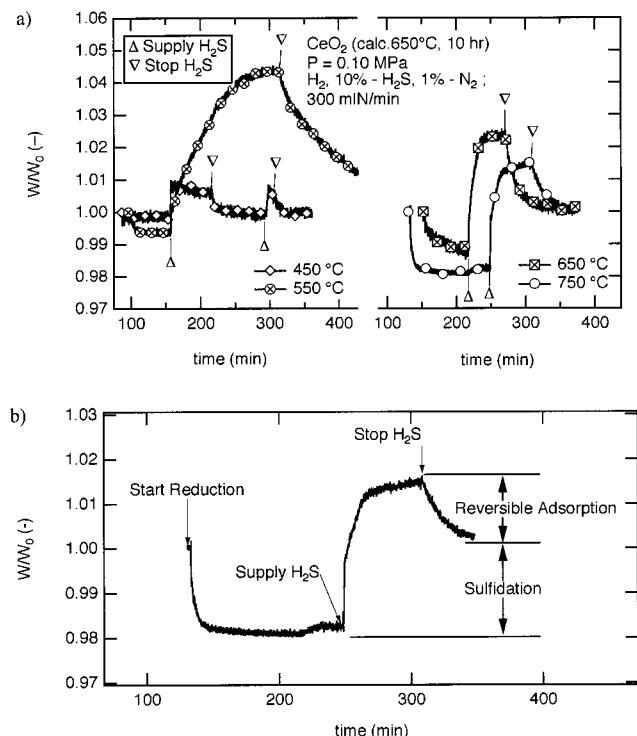


Figure 9. (a) Reduction and succeeding sulfidation profiles of CeO_2 followed by decomposition in 10% H_2 /(0 or 1%) $\text{H}_2\text{S}/\text{N}_2$ gas mixtures at various temperatures. (b) Same at 750 °C.

or clusters interacting with ceria.¹⁸ This is reflected by the high initial reduction rate of the sample. Also notable is the fact that all the Cu-containing ceria samples preserve nanoscale ceria even after the high-temperature calcination; see Table 2. Nanocrystalline ceria is known to contain a much larger concentration of oxygen defects than sintered ceria.⁴⁹

Interaction of Hydrogen Sulfide with Cerium Oxide. The adsorption of H_2S on prerduced ceria was studied by isothermal uptake experiments in the TGA. The adsorption kinetics can be derived from the uptake versus time plots of the isotherm for each H_2S concentration. Figure 9a shows H_2S uptake profiles in a 1% $\text{H}_2\text{S}/10\%$ H_2/N_2 gas mixture after reduction of ceria in 10% H_2/N_2 gas at the temperature of sulfidation. Each weight profile shows a relatively small, rapid weight increase immediately after the introduction of hydrogen sulfide. This is followed by a rather long slow weight increase.

Adsorption was followed by desorption in the 10% H_2/N_2 gas to examine its reversibility. Figure 9b is a detailed view of Figure 9a showing the full test of reduction/ H_2S adsorption/desorption at 750 °C. Desorption was performed right after the initial plateau of sulfur uptake was observed. When the supply of hydrogen sulfide was stopped, the sample weight decreased. The weight ratio W/W_0 after desorption converged to the value of unity that it had prior to reduction. This was true also for the other temperatures studied, as shown in Figure 9a, except for the 550 °C case. Thus, H_2S adsorption on ceria is partially reversible. The irreversible branch is attributed to sulfide formation. This may derive from dissociative chemisorption of H_2S , and filling by sulfur of the oxygen vacancies of ceria created by hydrogen reduction. This is the branch of very rapid initial weight increase in Figure 9a and b. This "sulfur capacity" increases with temperature. In this manner,

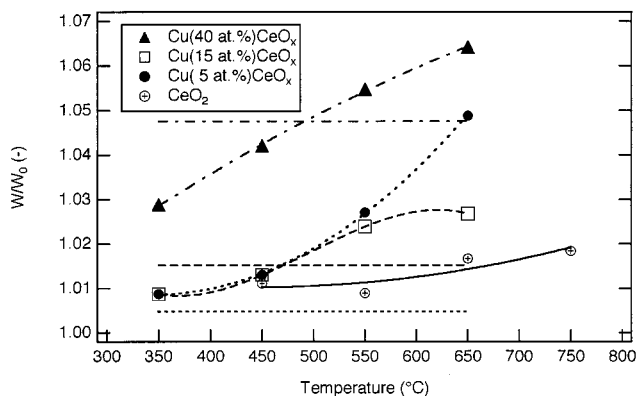


Figure 10. Weight increase due to sulfidation of prerduced Cu (5–40 atom %)- CeO_x after 300 s in a 1% $\text{H}_2\text{S}/10\%$ H_2/N_2 gas mixture at various temperatures.

the H_2S uptake of reduced ceria provides also a measure of the oxygen storage capacity of ceria at each temperature.

At 450 °C, almost no reduction takes place; see Figure 9a. However, a quick sulfidation to the W/W_0 value ~ 1.007 follows the introduction of H_2S . A second cycle of sulfur uptake reproduces the results of the first. At this temperature, mostly reversible adsorption occurs. The data for the other three temperatures indicate that adsorption is exothermic, with the total uptake decreasing with temperature. At 550 °C, the final sulfur uptake is reached much more slowly than it is at the other temperatures. This result was reproducible, but we cannot offer an explanation for it at this time.

Sulfidation of Cu-CeO_x. In this section we examine the sulfidation of prerduced Cu-CeO_x composite oxides. The sulfidation characteristics are analyzed under similar assumptions as those for the reduction analysis presented above. Thus, we will estimate the extent of ceria sulfidation by first determining the copper sulfidation. Figure 10 shows the normalized weight increase during an initial period of 300 s for each sorbent composition. The horizontal lines show the expected weight increase for complete sulfidation of the copper portion to form Cu_2S , which is the thermodynamically dominant phase at the experimental conditions of sulfidation. The oxide with the lowest copper concentration, 5 atom % Cu-CeO_x, clearly shows a contribution from the ceria portion at all temperatures, while the 15 atom % Cu-CeO_x sample shows such a contribution only above 550 °C.

It is not possible to specify the sulfidation products of ceria from the weight increase, which may be due to a combination of reactions 5–7. Furthermore, the coexistence of CeO_2 and reduced cerium oxide does not allow identification of sulfidation products and corresponding conversion. We can attempt to estimate the contribution of ceria, however, by considering the most plausible reactant and product of ceria sulfidation. The most plausible reactant on the basis of thermodynamics is Ce_2O_3 , not CeO_2 . At the given reaction condition, P_{S_2} is around -10.3 at 700 °C. The partial pressure of oxygen, P_{O_2} , is sufficiently low to reduce CeO_2 , which is supported by Figure 7. Thus, the stable sulfidation product is considered to be Ce_2S_3 on the basis of the phase diagram. This estimation is also applicable over the temperature range studied in Figure 10. In other

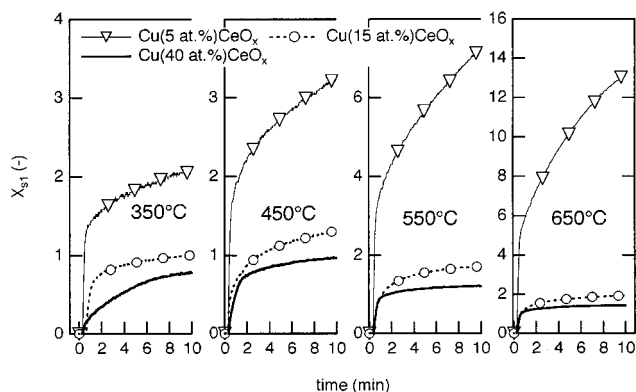


Figure 11. Conversion of Cu to Cu_2S in sulfidation of prereduced Cu– CeO_x samples at various temperatures (1% $\text{H}_2\text{S}/10\%$ H_2/N_2 , 500 mL of N_2/min , 0.1 MPa, 623–1023 K).

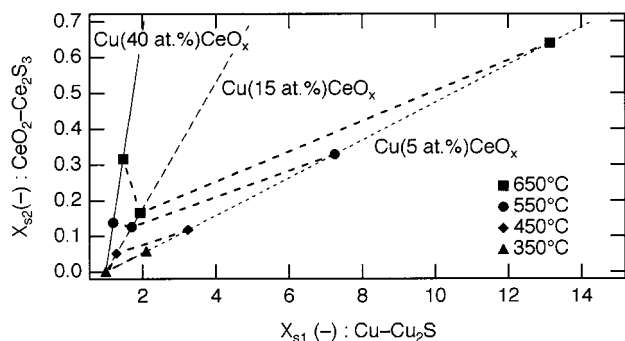


Figure 12. Estimated conversion of CeO_2 to Ce_2S_3 after 10 min of sulfidation of prereduced Cu– CeO_x samples at various temperatures.

work with Cu– CeO_x materials,¹⁶ the sulfide Ce_2S_3 was identified by XRD.

Figure 11 shows the conversion–time profiles of sulfidation of prereduced Cu–ceria samples during the initial 10 min of reaction. The conversion of copper, X_{s1} , is calculated assuming formation of Cu_2S . X_{s1} substantially exceeds unity; the excess sulfidation is attributed to a contribution from ceria, as discussed above. The conversion of ceria, X_{s2} , is shown in Figure 12, which shows the correlation between X_{s1} and X_{s2} for various sorbent compositions and temperatures after 10 min of sulfidation. The low-content 5 atom % Cu– CeO_x sample shows the highest X_{s2} at all temperatures. The resemblance to Figure 7, which shows the reduction conversion of ceria, is notable. If we compare X_{s2} to X_{r2} for the same temperature and reaction time, the former is always higher than the latter. This is true for all sample compositions. A plausible explanation for this is that further adsorption of H_2S takes place on the sulfided ceria.

Initial Sulfidation Reaction Rates of Copper-Containing Ceria and Pure Ceria. The initial sulfidation rates of the prereduced sorbents are shown in Figure 13, in Arrhenius-type plots. The rates are expressed in mmol H_2S adsorbed/gram sorbent/s. There are two main observations from this figure: first, the sulfidation rate of all the Cu-containing ceria samples is much higher than that of pure ceria, while the various Cu–ceria compositions cluster together. Data for the 50 atom % Cu– CeO_x sample from ref 16 are also included for comparison. While the sulfidation rate of this sample is higher, it should be noted that its prereduction took place at 750 °C.¹⁶ The other samples were all prereduced at the temperature of the ensuing sulfidation, as

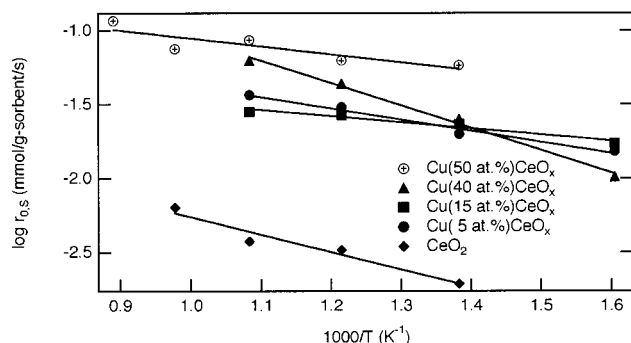


Figure 13. Arrhenius-type plot of the initial sulfidation rate of prereduced Cu (5–40 atom %)- CeO_x and CeO_2 powders (1% $\text{H}_2\text{S}/10\%$ H_2/N_2 , 500 mL of N_2/min , 0.1 MPa).

discussed above. Thus, a different sorbent structure is expected for the latter.

The second important observation from this figure is the similarity of the sulfidation reduction slope for all sorbents, including ceria. The only exception is the 40 atom % Cu–ceria sample. The deviation of the latter may be due to artificially lower sulfidation rates measured at the two lowest temperatures, because of incomplete reduction, as was established in Figures 5 and 6. If we properly correct for this, the slopes are very close for all sorbent compositions. The common sulfidation site in all sorbents is the reduced Ce_2O_3 site. The number of such sites increases in the presence of copper, which can explain the higher sulfidation rates of the Cu–ceria samples. We can also propose that the reduced cerium oxide site has faster sulfidation kinetics than those for metallic copper, on the basis of these results.

Sulfidation rate constants were calculated by assuming a power-law dependence of the rate on H_2S , $R_{s0} = k_s C_{\text{H}_2\text{S}}^n$. The reaction order n was determined from a series of tests performed at 823 K with H_2S content in the range 0.5–1.5%. The value 0.38 was thus obtained for n . Assuming that this value is independent of temperature, the Arrhenius constants can be calculated from $k_s = k_{s0} \exp(-E_a/RT)$. The apparent activation energy thus calculated was 16 ± 3 kJ/mol for all sorbents, except the 40% Cu–ceria. More detailed kinetic studies are underway to determine reaction orders at various temperatures and fit the data to a suitable reaction model.

Conclusions

Copper-containing cerium oxide materials were prepared by the urea coprecipitation/gelation method and tested in reduction and sulfidation in an ambient-pressure thermobalance reactor over the temperature range 623–923 K. H_2 -TPR and *in situ* X-ray diffraction analysis were applied to determine reduction temperature, extent of reduction, and reduction products of the Cu–ceria composite oxides with various copper contents. The main reduction product was metallic copper, which is readily produced below 473 K. In the presence of copper, CeO_2 is much more extensively reduced, which in turn helps to improve the sulfidation kinetics and sulfur capacity of ceria. The most pronounced effect was found with the low-Cu-content (5 atom %) sample. This material retains the smallest particle size of ceria (7.2 nm). A strong interaction of copper and ceria at the interface may be invoked to explain the increased reducibility of ceria at low temperatures. This correlates well with the increased sulfidation activity of the Cu–

ceria system. Our data indicate that the fast initial sulfidation reaction rate is that of reduced cerium oxide sites.

On the basis of these findings, a suitably modified cerium oxide with metal oxide additives can be reduced more extensively to the Ce(III) oxide form, which has a high sulfidation equilibrium constant. If the kinetics of sulfidation is also fast, such a formulation may be one of the most attractive H₂S sorbents, with a much wider operating temperature window than is currently considered possible for cerium oxide.

Acknowledgment

The financial support of M.K. by CRIEPI, Yokosuka Research Laboratory, during his tenure at Tufts University is gratefully acknowledged. The *in situ* XRD analysis performed at the Yokosuka Research Center is also appreciated.

Literature Cited

- (1) Tamhankar, S. S.; Hasatani, M.; Wen, C. Y. Kinetic-Studies on the Reactions Involved in the Hot Gas Desulfurization Using a Regenerable Iron-Oxide Sorbent. 1. *Chem. Eng. Sci.* **1981**, *36*, 1181.
- (2) Westmoreland, P. R.; Gibson, J. B.; Harrison, D. P. Comparative Kinetics of High-Temperature Reaction between H₂S and Selected Metal-Oxides. *Environ. Sci. Technol.* **1977**, *11*, 488.
- (3) Furimsky, E.; Yumura, M. Solid Adsorbents for Removal of Hydrogen-Sulfide from Hot Gas. *Environ. Sci. Technol.* **1986**, *20*, 163.
- (4) Grindley, T.; Steinfeld, G. *Development and Testing of Regenerable Hot Coal Gas Desulfurization Sorbents*; Final Report DOE/MC/16545-1125; Oct. 1981.
- (5) Lew, S.; Sarofim, A. F.; Flytzani-Stephanopoulos, M. Sulfidation of Zinc Titanate and Zinc-Oxide Solids. *Ind. Eng. Chem. Res.* **1992**, *31*, 1890.
- (6) Focht, G. D.; Ranade, P. V.; Harrison, D. P. High-Temperature Desulfurization Using Zinc Ferrite—Reduction and Sulfidation Kinetics. *Chem. Eng. Sci.* **1988**, *43*, 3005.
- (7) Patrick, V.; Gavalas, G. R.; Flytzani-Stephanopoulos, M.; Jothimurugesan, K. High-Temperature Sulfidation Regeneration of Cuo-Al₂O₃ Sorbents. *Ind. Eng. Chem. Res.* **1989**, *28*, 931.
- (8) Barin, I.; Sauert, F.; Schultze-Rhonhof, E.; Sheng, W. S. *Thermochemical Data of Pure Substances Part I, Part II*; VCH: Weinheim, Germany, 1993.
- (9) Barin, I.; Knacke, O. *Thermochemical Properties of Inorganic Substances*; Springer-Verlag: New York, 1973. Barin, I.; Knacke, O.; Kubaschewski, O. *Thermochemical Properties of Inorganic Substances*; Springer-Verlag: New York, 1977; Supplement.
- (10) Lew, S.; Sarofim, A. F.; Flytzani-Stephanopoulos, M. The Reduction of Zinc Titanate and Zinc Oxide Solids. *Chem. Eng. Sci.* **1992a**, *47*, 1421–1431.
- (11) Lew, S. High-Temperature Sulfidation and Reduction of Zinc Titanate and Zinc Oxide Sorbents. Ph.D. Dissertation, MIT, Cambridge, MA, 1990.
- (12) Flytzani-Stephanopoulos, M.; Yu, T. U.; Lew, S. *Development and Testing of Desulfurization Sorbents*; Topical Report to Texaco, under Subcontr. DOE Coop. Agreement No. DE-FC21-87MC23277; Dec. 1988.
- (13) Mei, J. S.; Gasper-Galvin, L.; Everitt, C. E.; Katta, S. *Proceedings of the Coal-fired Power Systems 93—Advances in IGCC and PFBC Review Mtg*; DOE/METC-93/6131; June 1993; pp 315–325.
- (14) Tamhankar, S. S.; Bagajewicz, M. J.; Gavalas, G. R.; Sharma, P. K.; Flytzani-Stephanopoulos, M. Mixed-Oxide Sorbents for High-Temperature Removal of Hydrogen-Sulfide. *Ind. Eng. Chem. Process Des. Dev.* **1986**, *25*, 429–37.
- (15) Abbasian, J.; Hill, A. H.; Li, Z.; Flytzani-Stephanopoulos, M. *Development of novel copper-based sorbents for hot-gas cleanup*. IGT-Final Report to ICCI/DOE, DE-FC22-92PC92521; Aug. 1994.
- (16) Li, Z.; Flytzani-Stephanopoulos, M. Cu–Cr–O and Cu–Ce–O regenerable oxide sorbents for hot gas desulfurization. *Ind. Eng. Chem. Res.* **1997**, *36*, 187.
- (17) Liu, W.; Flytzani-Stephanopoulos, M. Transition metal-promoted oxidation catalysis by fluorite oxides: A study of CO oxidation over Cu–CeO₂. *Chem. Eng. J.* **1996**, *64*, 283.
- (18) Kundakovic, Lj.; Flytzani-Stephanopoulos, M. Reduction characteristics of copper oxide in cerium and zirconium oxide systems. *Appl. Catal. A* **1998**, *171*, 13.
- (19) Kay, D. A. R.; Wilson, W. G. Desulfurization of fluid materials. U.S. Patent No. 4,507,149, 1985.
- (20) Kay, D. A. R.; Wilson, W. G. Regeneration of cerium oxide from sulfur-containing cerium compounds formed in desulfurization of sulfur-containing fluids with cerium oxide. U.S. Patent No. 4,826,664, 1989.
- (21) Wilson, W. G. *Superior method for desulfurization of low and medium Btu Gas*; Final Report, DOE/SBIR Contr. # DE-AC01-86ER80347.
- (22) Zeng, Y.; Zhang, S.; Groves, F. R.; Harrison, D. P. High-temperature gas desulfurization with elemental sulfur production. *Chem. Eng. Sci.* **1999**, *54* (15), 3007.
- (23) Meriani, S. Features of the Caeria Zirconia System. *Mater. Sci. Eng. A* **1989**, *109*, 121.
- (24) Trovarelli, A. Catalytic properties of ceria and CeO₂-containing materials. *Catal. Rev.—Sci. Eng.* **1996**, *38*, 439.
- (25) Gandhi, H. S.; Piken, A. G.; Shelef, M.; Delosh, R. G. SAE Paper 760201; 1976; p 55.
- (26) Yao, H. C.; Yu Yao, Y. F. Ceria in Automotive Exhaust Catalysts. 1. Oxygen Storage. *J. Catal.* **1984**, *86*, 254.
- (27) Jen, H. W.; Graham, G. W.; Chun, W.; McCabe, R. W.; Cuif, J. P.; Deutsch, S. E.; Touret, O. Characterization of model automotive exhaust catalysts: Pd on ceria and ceria-zirconia supports. *Catal. Today* **1999**, *50*, 309.
- (28) Sharma, S.; Hilaire, S.; Vohs, J. M.; Gorte, R. J.; Jen, H. W. Evidence for oxidation of ceria by CO₂. *J. Catal.* **2000**, *190*, 199.
- (29) Li, Y.; Fu, Q.; Flytzani-Stephanopoulos, M. Low-temperature water-gas shift reaction over Cu- and Ni-loaded cerium oxide catalysts. *Appl. Catal. B* **2000**, *27*, 179.
- (30) Fu, Q.; Weber, A.; Flytzani-Stephanopoulos, M. Nanostructured Au–CeO₂ catalysts for low-temperature water-gas shift. *Catal. Lett.* **2001**, *77*, 87.
- (31) Fu, Q.; Kudriavtseva, S.; Saltsburg, H.; Flytzani-Stephanopoulos, M. Gold-ceria Catalysts for Low-Temperature Water-gas Shift Reaction. *Chem. Eng. J.*, in press.
- (32) Liu, W.; Wadia, C.; Flytzani-Stephanopoulos, M. Transition metal/fluorite-type oxides as active catalysts for reduction of sulfur dioxide to elemental sulfur by carbon monoxide. *Catal. Today* **1996**, *28*, 391.
- (33) Flytzani-Stephanopoulos, M.; Zhu, T.; Li, Y. Ceria-based catalysts for the recovery of elemental sulfur from SO₂-laden gas streams. *Catal. Today* **2000**, *62*, 145.
- (34) Zhu, T.; Flytzani-Stephanopoulos, M. Catalytic partial oxidation of methane to synthesis gas over Ni–CeO₂. *Appl. Catal. A* **2001**, *208*, 403.
- (35) Hilaire, S.; Wang, X.; Luo, T.; Gorte, R. J.; Wagner, J. A comparative study of water-gas-shift reaction over ceria supported metallic catalysts. *Appl. Catal. A* **2001**, *215* (1–2), 271.
- (36) Amenomiya, Y.; Emesh, A.; Oliver, K.; Pleizer, G. Copper–zirconium oxide catalysts for the synthesis and dehydrogenation of methanol. In *Proceedings of the Ninth International Congress on Catalysis*; Phillips, M., Ternan, M., Eds.; Chemical Institute of Canada: Ottawa, Canada, 1988.
- (37) Sick, G.; Schwerdtfeger, K. Hot Desulfurization of Coal-Gas with Copper. *Metall. Trans. B* **1987**, *18B*, 603.
- (38) Sick, G.; Schwerdtfeger, K. Kinetics of Formation at 800-Degrees-C of Cu₂S on Copper under Gases Containing H₂S. *Mater. Sci. Technol.* **1986**, *2*, 159.
- (39) Swisher, J. H.; Schwerdtfeger, K. Review of Metals and Binary Oxides as Sorbents for Removing Sulfur from Coal-Derived Gases. *J. Mater. Eng. Perform.* **1992**, *1*, 399.
- (40) Meng, V. V.; Kay, D. A. R. Gaseous desulfurization using rare earth oxides. In *High Technology Ceramics*; Vincenzini, P., Eds.; Elsevier: Amsterdam, 1987.
- (41) Dwivedi, R. K.; Kay, D. A. R. Determination of the Standard Free-Energies of Formation of Ce₂O₂S and Y₂O₂S at High-Temperatures. *J. Less-Common Met.* **1984**, *102*, 1.
- (42) Klug, H. P.; Alexander, L. E. *X-ray Diffraction Procedure for Polycrystalline and Amorphous Materials*; Wiley-Interscience Publ.: New York, 1974.

- (43) Bera, P.; Aruna, S. T.; Patil, K. C.; Hegde, M. S. Studies on Cu/CeO₂: A new NO reduction catalyst. *J. Catal.* **1999**, *186*, 36.
- (44) Liu, W.; Flytzani-Stephanopoulos, M. Total Oxidation of Carbon-Monoxide and Methane over Transition Metal-Fluorite Oxide Composite Catalysts. 2. Catalyst Characterization and Reaction-Kinetics. *J. Catal.* **1995**, *153*, 317.
- (45) Kundakovic, Lj. Complete Oxidation of Methane over Ag- and Cu-Modified Cerium and Zirconium Oxides. Ph.D. Dissertation, Department of Chemical Engineering, Tufts University, 1998.
- (46) Gregg, S. J.; Sing, K. S. W. *Adsorption, Surface Area and Porosity*, 2nd ed.; Academic Press: London, U.K., 1982.

- (47) Newmann, R. A.; Blazy, J. A.; Fawcett, T. G.; Whiting, L. F.; Stowe, R. A. *Adv. X-Ray Anal.* **1987**, *30*, 493.
- (48) Qi, X. Ph.D. Thesis, Tufts University, in progress.
- (49) Chiang, Y. M.; Lavik, E. B.; Kosacki, I.; Tuller, H. L.; Ying, J. Y. Nonstoichiometry and Electrical Conductivity of Nanocrystalline CeO_{2-x}. *J. Electroceram.* **1997**, *1*, 7.

Received for review October 2, 2001
Revised manuscript received April 18, 2002
Accepted April 19, 2002

IE010815W